

Rayleigh–Bénard instability in a vertical cylinder with a rotating magnetic field

J.S. Walker^{a,*}, M.P. Volz^b, K. Mazuruk^b

^a *Department of Mechanical and Industrial Engineering, University of Illinois, 1206 West Green Street, Urbana, IL 61801, USA*

^b *NASA Marshall Space Flight Center, SD 46, Huntsville, AL 35812, USA*

Received 2 May 2003; received in revised form 1 October 2003

Abstract

This paper presents a linear stability analysis for the Rayleigh–Bénard convection in a finite-length, vertical cylinder with a rotating magnetic field. The vertical wall of the cylinder is adiabatic, and the planar top and bottom walls are isothermal with a higher temperature at the bottom. The stabilizing effects of the rotating magnetic field are studied for four values of the Prandtl number. Results for one Prandtl number are compared to previously published experimental results.

© 2003 Elsevier Ltd. All rights reserved.

1. Introduction

During the growth of a single crystal from a body of a molten semiconductor or melt, hydrodynamic instabilities often lead to periodic melt motions. The resultant fluctuations in the convective heat transfer from the melt to the crystal lead to fluctuations in the rate of solidification. A fluctuating solidification rate produces more crystal defects and produces spatial oscillations of the dopant concentration in the crystal, called striations. Recent experiments have shown that the application of a rotating magnetic field (RMF) to the melt during crystal growth can dramatically improve the quality of the crystal. An RMF can have many beneficial effects, such as modifying the convective heat transfer to produce a more planar crystal-melt interface and stirring the melt to produce a more radially uniform dopant concentration in the crystal. This paper is focused on the use of an RMF to eliminate a hydrodynamic instability. Dold and Benz [1] presented an excellent review of the benefits of RMF's in semiconductor crystal growth.

An RMF is produced by connecting the successive phases of a multiphase AC power source to inductors at

equally spaced azimuthal positions around the cylindrical melt. A “high-frequency” RMF induces electric currents in the electrically conducting melt, and these currents produce an “induced” magnetic field which partially cancels the “applied” magnetic field due to the external inductors. The definition of high frequency depends on the electrical conductivity σ of the melt and the radius R of the melt region. For virtually all molten semiconductors with $R \leq 10$ cm, 50 or 60 Hz is a “low frequency”, and the induced magnetic field is negligible [2–4]. While higher frequencies are certainly possible, modeling indicates that they lead to undesirable instabilities [5].

For most crystal-growth processes, the inductors are designed to produce a spatially uniform, transverse magnetic field which rotates at a constant angular velocity ω around the vertical centerline of the melt region. While the induced electric currents in the melt are too small to produce a significant induced magnetic field, they are large enough to interact with the RMF to produce a significant electromagnetic body force on the melt. This body force consists of a steady, axisymmetric, azimuthal force and a periodic, three-dimensional force which varies as $\cos(2\theta)$ and which has a frequency of 2ω , where r, θ, z are cylindrical coordinates with the z axis along the vertical centerline of the melt region. If the frequency is too low, e.g., 0.1 Hz, then the melt can respond to the three-dimensional, periodic,

* Corresponding author. Tel.: +1-217-333-7979; fax: +1-217-244-6534.

E-mail address: jswalker@uiuc.edu (J.S. Walker).

Nomenclature

b	aspect ratio
B	magnetic flux density
f_{θ}	body force due to RMF
g	acceleration of gravity
J_k	Bessel function of k th order
m	azimuthal wave number
p	pressure
Pr	Prandtl number
r	radial coordinate
R	radius of cylinder
Ra	Rayleigh number
t	time
T	temperature
T_m	magnetic Taylor number
\mathbf{v}	velocity
z	axial coordinate

Greek symbols

β	volumetric expansion coefficient
ε	small parameter for perturbation
θ	azimuthal coordinate
κ	thermal diffusivity
λ	complex eigenvalue
λ_N	roots of $\lambda_N J_0(\lambda_N) - J_1(\lambda_N) = 0$
ν	kinematic viscosity
ρ	density
σ	electrical conductivity
Φ	azimuthal phase shift
ψ	stream function for meridional flow
ω	angular velocity of RMF
Ω_0	angular velocity of flow

nonaxisymmetric component of the RMF body force, leading to an undesirable melt motion [6]. For a frequency of 50 or 60 Hz, the melt motion driven by the three-dimensional, periodic, nonaxisymmetric component of the RMF body force is limited by inertial effects and is negligible compared to the melt motion driven by the steady, axisymmetric, azimuthal component of the RMF body force [7–9]. The assumptions needed for the neglect of the three-dimensional, periodic, nonaxisymmetric component of the RMF body force also indicate that the steady, axisymmetric, azimuthal component is independent of the melt motion [9].

Volz and Mazuruk [10] recently presented an experimental study of the influence of a rotating magnetic field on the Rayleigh–Bénard instability in a vertical cylinder with a well-insulated vertical wall, with isothermal planar top and bottom walls with a hotter bottom, and with its height equal to its diameter. The liquid gallium in their experiments has a Prandtl number $Pr = \nu/\kappa = 0.0285$ and other thermophysical properties which are close to those of many molten semiconductors, where ν and κ are the kinematic viscosity and thermal diffusivity of the melt. Without an RMF, the Rayleigh–Bénard base-state consists of a stagnant fluid with a linear temperature variation from the hot bottom to the cold top. In this case, the first instability as the temperature difference is increased involves the transition to a steady axisymmetric or nonaxisymmetric flow. If the cylinder is rotated about its vertical centerline, the base-state consists of a rigid body rotation with the cylinder and a linear temperature variation, with the initial transition to an axisymmetric or nonaxisymmetric flow which is steady in a reference frame rotating with

the cylinder [11]. For a fixed, finite-length cylinder with a rotating magnetic field, the base-state consists of (1) the azimuthal velocity $v_{\theta 0}(r, z)$ driven by the RMF, (2) a meridional circulation which consists of radial and axial velocity components and which is driven by the axial variation of the centrifugal force due to $v_{\theta 0}$, and (3) a temperature which deviates from a linear variation due to the convective heat transfer associated with the base-state meridional circulation. Here we only treat the first transition from a steady, axisymmetric velocity and temperature to a periodic axisymmetric or nonaxisymmetric velocity and temperature. Volz and Mazuruk [12] also presented a linear stability analysis for an infinitely long vertical cylinder with a base-state consisting of a uniform temperature gradient and an azimuthal velocity due to an RMF.

2. Problem formulation

With the Boussinesq approximation, the dimensionless governing equations are

$$\frac{\partial \mathbf{v}}{\partial t} + (\mathbf{v} \cdot \nabla) \mathbf{v} = -\nabla p + T_m f_{\theta}(r, z) \hat{\theta} + \frac{Ra}{Pr} T \hat{\mathbf{z}} + \nabla^2 \mathbf{v}, \quad (1)$$

$$\nabla \cdot \mathbf{v} = 0, \quad (2)$$

$$\frac{\partial T}{\partial t} + \mathbf{v} \cdot \nabla T = \frac{1}{Pr} \nabla^2 T, \quad (3)$$

where (1) the coordinates r and z are normalized by R , (2) t is the time normalized by R^2/ν , (3) \mathbf{v} the liquid velocity normalized by ν/R , (4) p the deviation of the pressure from the hydrostatic pressure for a uniform

density ρ , normalized by $\rho v^2/R^2$, (5) T the deviation of the temperature from $0.5(T_h + T_c)$, normalized by $(\Delta T) = T_h - T_c$, while T_h and T_c are the uniform temperatures of the hot bottom wall and cold top wall, respectively, and (6) $\hat{\mathbf{r}}$, $\hat{\theta}$, $\hat{\mathbf{z}}$ are unit vectors for the cylindrical coordinates. In addition to Pr , the dimensionless parameters are the magnetic Taylor number

$$T_m = \frac{\sigma \omega B^2 R^4}{2\rho v^2} \tag{4}$$

and the Rayleigh number

$$Ra = \frac{g\beta(\Delta T)R^3}{\nu\kappa}, \tag{5}$$

where B is the magnetic flux density of the RMF, $g = 9.81 \text{ m/s}^2$, and β is the volumetric expansion coefficient of the liquid. The dimensionless, steady, axisymmetric, azimuthal body force f_θ produced by the RMF depends on the electrical conductivity of the top and bottom walls. If the top and bottom walls are perfect electrical conductors, then $f_\theta = r$ [7]. In the experiments of Volz and Mazuruk [10], the top and bottom walls were copper disks, and a thin oxide layer formed at each copper–gallium interface. These oxide layers are electrically insulating. With the origin of the coordinate system at the middle of the liquid, the solution for the RMF body force for electrically insulating top and bottom walls is [9]

$$f_\theta = r - 2 \sum_{N=1}^{\infty} \frac{J_1(\lambda_N r) \cosh(\lambda_N z)}{(\lambda_N^2 - 1) J_1(\lambda_N) \cosh(\lambda_N b)}, \tag{6}$$

where J_k is the Bessel function of the first kind and k th order, λ_N are the roots of $\lambda_N J_0(\lambda_N) - J_1(\lambda_N) = 0$, and b is the ratio of the axial distance between the top and bottom walls of the cylinder to its diameter. The boundary conditions are

$$\mathbf{v} = 0, \quad \frac{\partial T}{\partial r} = 0, \quad \text{at } r = 1, \tag{7}$$

$$\mathbf{v} = 0, \quad T = \mp 0.5, \quad \text{at } z = \pm b. \tag{8}$$

For the linear stability analysis, we introduce the form

$$v_r = v_{r0}(r, z) + \varepsilon \text{Real}[v_{r1}(r, z) \exp(\lambda t - im\theta)] \tag{9}$$

for each of the variables v_r, v_θ, v_z, p, T . Here the subscript 0 denotes the variables in the steady, axisymmetric base-flow, the subscript 1 denotes the complex modal functions, such as $v_{r1} = v_{r1R} + iv_{r1I}$, for the small $O(\varepsilon)$ perturbation in the linear stability analysis, $\lambda = \lambda_R + i\lambda_I$ is the complex eigenvalue, and m is the real, integer, azimuthal wave number. The base-flow and linear-perturbation equations neglect $O(\varepsilon)$ and $O(\varepsilon^2)$ terms, respectively.

For the steady, axisymmetric base-flow, we introduce a stream function $\psi_0(r, z)$ for the meridional circulation, where

$$v_{r0} = \frac{1}{r} \frac{\partial \psi_0}{\partial z}, \quad v_{z0} = -\frac{1}{r} \frac{\partial \psi_0}{\partial r}, \tag{10}$$

and we eliminate p_0 by cross-differentiating the r and z components of the momentum equation (1). Thus the base-flow is governed by a fourth-order equation for ψ_0 and two second-order equations governing $v_{\theta 0}$ and T_0 . Since $v_{\theta 0}$ is an even function of z , while ψ_0 and T_0 are odd functions of z , we need only treat $0 \leq z \leq b$. We represent each base-flow variable by a sum of the Chebyshev polynomials in r and z . We insure that the representation of each variable has the correct Taylor series in r . For example, the Taylor series for ψ_0 has only even powers of r , starting with r^2 . We apply each equation and boundary condition at the Gauss–Lobatto collocation points in r and z , including $r = 0$ and $z = 0$. For each equation at $r = 0$, we identify the leading power of r in the Taylor series of that equation, we divide by this power of r , and we take the limit as $r \rightarrow 0$. For an equation which is odd in z , we apply its z -derivative at $z = 0$. For each combination of the parameters b, Pr, T_m, Ra , the nonlinear base-flow equations are solved with an iterative Newton–Raphson scheme.

The complex modal functions $v_{r1}, v_{\theta 1}, v_{z1}, p_1, T_1$ are governed by a set of linear, homogeneous equations and boundary conditions which involve coefficients given by the base-flow variables and their first derivatives and which include the complex eigenvalue λ . Since the base-flow has a symmetry in z , we need only treat $0 \leq z \leq b$ as long as we consider both symmetric and antisymmetric modes. A symmetric mode has the same symmetries as the base-flow: $v_{r1}, v_{\theta 1}, p_1$ are even functions of z , and v_{z1}, T_1 are odd functions of z . For an antisymmetric mode: $v_{r1}, v_{\theta 1}, p_1$ are odd functions of z , and v_{z1}, T_1 are even functions of z . In addition, different approaches are appropriate for an axisymmetric perturbation with $m = 0$ and for a nonaxisymmetric perturbation with $m \geq 1$. For $m = 0$, we introduce a stream function for the perturbation meridional circulation, corresponding to Eq. (10) with the subscript 0 replaced by the subscript 1. Then the three basic variables are $\psi_1, v_{\theta 1}, T_1$. For $m \geq 1$, we use the continuity Eq. (2) to eliminate $v_{\theta 1}$ and then we use the θ component of the momentum equation (1) to eliminate p_1 , so that we have fourth-order equations governing v_{r1}, v_{z1} and a second-order equation governing T_1 . We have developed four codes for the symmetric and antisymmetric modes with $m = 0$ and $m \geq 1$.

Each perturbation variable is represented as a sum of Chebyshev polynomials in r and z , and again we insure that each representation has the correct Taylor series in r . For example, the Taylor series for v_{r1} for $m \geq 1$ includes only the powers $r^{(m-1)}, r^{(m+1)}, r^{(m+3)}, r^{(m+5)}, \dots$ The

perturbation equations are also applied at the Gauss–Lobatto collocation points in r and z , including $r = 0$ and $z = 0$. Again the leading term in the Taylor series expansion of each equation is applied at $r = 0$, and the derivatives of equations which are odd in z are applied at $z = 0$.

The resultant linear matrix eigenvalue problem was solved with two methods. First we obtained approximate values for all the eigenvalues with a relatively small number of collocation points for the perturbation equations using the FORTRAN subroutines in the EISPACK library [13]. Then we used the inverse iteration method [14] with more collocation points in both the r and z directions in order to obtain much more accurate eigenvalues and eigen vectors for all potentially critical modes.

For each set of values for b , Pr , T_m , Ra , we first used the Newton–Raphson scheme to determine the steady, axisymmetric base-flow, and then we found the eigenvalues for the symmetric and antisymmetric modes for $m = 0, 1, 2, 3, 4, \dots$. For each set of values of b , Pr , T_m , we increased Ra until one eigenvalue for one mode had $\lambda_R = 0$, while all the other eigenvalues for this mode and for all the other modes had $\lambda_R < 0$.

3. Results

We only present results for $b = 1$ because this is the aspect ratio for the experiments of Volz and Mazuruk [10]. Grid refinement studies indicated that 31 and 47 collocation points in $0 \leq r \leq 1$ and $0 \leq z \leq 1$, respectively, provided accurate results for all the cases considered here. Further validation of the numerical accuracy was provided by comparison with previous results for two special cases. For the Rayleigh–Bénard instability without an RMF ($T_m = 0$), the initial transition from a stagnant fluid to a steady convection ($\lambda_1 = 0$) occurs at a critical value of the Rayleigh number, Ra_{cr} , which is independent of Pr . For $b = 1$, the critical mode is the antisymmetric $m = 1$ mode. Using linear stability analyses, Buell and Catton [11] found that $Ra_{cr} = 471$, while Touihri et al. [15] found that $Ra_{cr} = 462$. Using a numerical time integration of the full three-dimensional Navier–Stokes and energy equations, Neumann [16] found that $Ra_{cr} = 451$. Our codes give $Ra_{cr} = 471$. For an isothermal liquid ($Ra = 0$) in a cylinder with an RMF, Grants and Gerbeth [17] found a transition from a steady, axisymmetric flow to a periodic, nonaxisymmetric flow at $T_{mcr} = 123,200$ for $b = 1$. The critical mode is the symmetric $m = 2$ mode with $\lambda_1 = 160.42$. Our codes give $T_{mcr} = 123,168$ with $\lambda_1 = 160.422$.

There are three possible sources of instability: the Rayleigh–Bénard instability due to the temperature gradient, a centrifugal (Görtler) instability near the vertical cylinder wall, and a critical-layer instability in

the Bödewadt layers adjacent to the top and bottom walls. The Görtler and Bödewadt instability mechanisms are the same in the problem of an isothermal liquid in a cylinder with an RMF, which was treated by Grants and Gerbeth [17]. They showed that the first instability arises from a coupling of the Görtler and Bödewadt instability mechanisms in the regions near the corners at $r = 1$, $z = \pm b$. They found that this coupled instability occurs at $T_{mcr} = 123,200$ for $b = 1$, and they thoroughly documented their numerical accuracy. Here we consider $T_{mcr} \leq 70,000$, so we are only considering the modification of the Rayleigh–Bénard instability, and we are well below the value of T_m where the Görtler or Bödewadt instability mechanisms would enter.

For all the results presented here, the critical instability involves an antisymmetric mode with $m = 0, 1, 2$ or 3. For gallium with $Pr = 0.0286$, Ra_{cr} is plotted as a function of T_m in Fig. 1. The solid lines are the values of Ra_{cr} from the linear stability analysis for the $m = 1, 0$ and 2 antisymmetric modes. As T_m is increased from 0, Ra_{cr} for the $m = 1$ mode increases from 471.0 to 5016.0

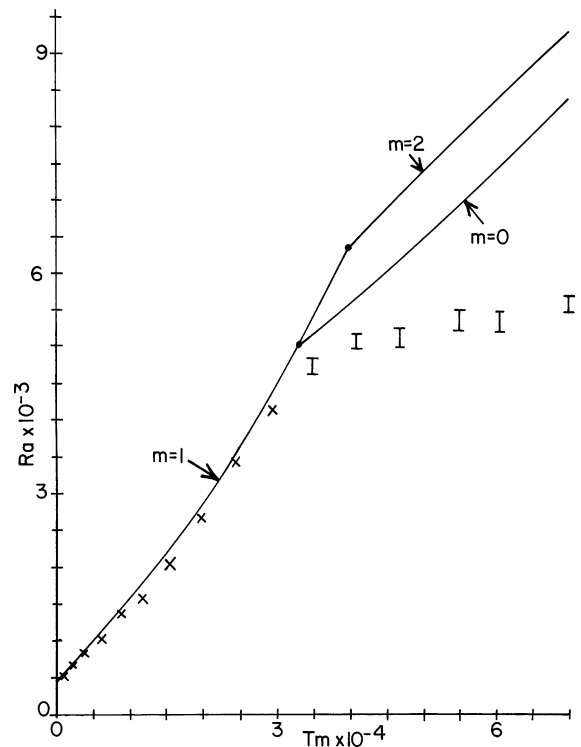


Fig. 1. Critical Rayleigh number versus magnetic Taylor number for gallium ($Pr = 0.0286$). The solid lines are the results of the linear stability analysis for the antisymmetric $m = 1, 0$ and 2 modes. The X's and I's are the experimental results of Volz and Mazuruk [10] for transitions from steady flows to periodic flows with azimuthal temperature variations corresponding to the $m = 1$ and 2 modes, respectively.

at $T_m = 33,000$, where the $m = 0$ mode becomes the first instability. In addition to the Ra_{cr} for the critical $m = 0$ mode, we continue to plot the Ra_{cr} for the $m = 1$ mode until it crosses the neutral stability curve for the $m = 2$ mode at $T_m = 39,630$ and $Ra_{cr} = 6325$. At $T_m = 70,000$, $Ra_{cr} = 8381.4$ and 9317.7 for the $m = 0$ and 2 modes, respectively.

In the experiments of Volz and Mazuruk [10], the temperature difference between the top and bottom copper disks was increased in small increments for each value of T_m . Each temperature difference was held constant for a long period of time before the temperatures at four equally spaced azimuthal positions were measured in order to determine whether the flow was steady or periodic. For $T_m < 70,000$, there were transitions from steady flow to two different periodic flows, with the azimuthal temperature variations corresponding to the $m = 1$ and 2 modes. The X's in Fig. 1 denote the last values of Ra before transition to the $m = 1$ temperature pattern as Ra was increased. The agreement with the linear stability predictions for the $m = 1$ mode is excellent. In these experiments, the incremental increases in (ΔT) were small, but they corresponded to significant changes in Ra since an increase of 1 K corresponds to an increase of 484 in Ra for gallium with $R = 12$ mm. Thus the first values of Ra where periodic flow occurred were above the values marked by the X's in Fig. 1. For example, for $T_m = 29,455$, the X marking the last Ra for steady flow lies at 4113.0, while the incremental temperature increase corresponded to roughly an increase of 250 in Ra . Therefore the first observed periodic flow occurred at roughly $Ra = 4363$, which lies very close to the solid line.

The I's in Fig. 1 denote the experimental results for the transitions between steady axisymmetric flows and periodic flows with an $m = 2$ azimuthal temperature variation. In the experiments of Volz and Mazuruk [10], for each value of T_m , Ra was first increased well beyond the transition from steady to periodic flow and then was decreased until the flow again became steady. The bottom of each I in Fig. 1 denotes the last value of Ra where steady flow was observed when Ra was increasing, and the top of each I denotes the last value of Ra where periodic flow was observed when Ra was decreasing. Clearly the experimental results for the transitions between steady and periodic flow with an $m = 2$ azimuthal temperature pattern are below the linear stability results for both the $m = 0$ and 2 modes. There are two characteristics of the linear stability results which support a hypothesis about the physical reason for the differences between the I's and the solid lines in Fig. 1. First, for the $Ra = 5000$ – 5500 for the I's, the dimensionless decay rates ($-\lambda_R$) for both the $m = 0$ and 2 modes are small compared to the dimensionless frequencies λ_1 . This indicates that a finite-amplitude disturbance would oscillate many times before decaying. Second the value

of λ_1 for the $m = 2$ mode is close to twice the value of λ_1 for the $m = 0$ mode. The ratio of these λ_1 's varies from 2.12 at $T_m = 42,000$ to 2.14 at $T_m = 70,000$. A ratio of two means that the period for one complete revolution of the $m = 2$ perturbation pattern is equal to the period for the oscillatory axisymmetric perturbation. These two characteristics lead to the hypothesis that a nonlinear coupling between the $m = 0$ and 2 periodic modes may lead to a transition from steady to periodic flow at a value of Ra below those predicted by the linear stability analysis for either mode. Finite-amplitude, axisymmetric ($m = 0$), antisymmetric (in z) perturbations would occur in any actual flow. While the linear stability analysis indicates that such a perturbation eventually decays for the values of Ra for the I's in Fig. 1, we hypothesize that such a perturbation could persist long enough to alter the steady base-flow, leading to a lower value of Ra_{cr} for the $m = 2$ mode. With the close match of the natural frequencies of the $m = 0$ and 2 modes, a periodic, axisymmetric, antisymmetric perturbation would certainly tend to drive the $m = 2$ mode. Of course this is only a hypothesis since such a nonlinear modal coupling cannot be treated with our linear stability analysis.

The experimentally measured frequencies for the periodic temperature oscillations at the top of each I in Fig. 1 are reasonably close to the frequencies predicted by the linear stability analysis for the neutral stability of the $m = 2$ mode at the same value of T_m . For example, for $T_m = 40,927$, $\lambda_1 = 671.65$ for a neutrally stable $m = 2$ mode, while the experimental frequency is equivalent to $\lambda_1 = 616.3$ or 8.2% less. There are many possible sources of a finite-amplitude, axisymmetric, antisymmetric perturbation which could alter the base-flow enough to trigger the $m = 2$ modal transition. One candidate is the convective heat transfer due to the base-flow meridional circulation produced by the RMF. Even for $Pr = 0.0286$, this convective heat transfer leads to a significant radial variation of the axial heat flux at either the top or bottom. For example, for $T_m = 60,000$, the axial heat flux at each interface at $r = 1$ is 62% larger than that at $r = 0$. For the idealized conditions of the model, the effects would be entirely symmetric in z . However, a small deviation from the idealized conditions could lead to a finite-amplitude, axisymmetric, antisymmetric perturbation. For example, if the thermal resistance of the oxide layer at the hotter copper–gallium interface were larger than that at the colder interface, the differences in temperature drops across these oxide layers would lead to an antisymmetric perturbation.

Volz and Mazuruk [12] presented a linear stability analysis for an infinitely long cylinder with a base-state consisting of a uniform axial temperature gradient and a purely azimuthal velocity driven by an RMF. Their results for $Pr = 0.02$ are qualitatively similar to the lines for $m = 1$ and 0 in Fig. 1. For the infinite cylinder with $T_m = 0$, Ra_{cr} for the $m = 1$ mode is below that for the

$m = 0$ mode. As T_m is increased from 0, the azimuthal velocity stabilizes the $m = 1$ mode, increasing its Ra_{cr} , but it has no effect on the $m = 0$ mode. Thus the roughly parabolically increasing Ra_{cr} for the $m = 1$ mode crosses the constant Ra_{cr} for the $m = 0$ mode, leading to a modal switch similar to that in Fig. 1 at $T_m = 33,000$.

The predictions of our linear stability analysis for Ra_{cr} for $Pr = 0.001, 0.0286, 0.2$ and 1.0 are plotted as functions of T_m in Fig. 2. For $T_m > 0$, there is a strong dependence of Ra_{cr} on Pr . First we discuss the differences in modal changes for the four values of Pr . For $Pr = 0.001$, the critical mode is the antisymmetric $m = 1$ mode with Ra_{cr} increasing from 471.0 to 2504.2 for $T_m = 70,000$. The neutral stability curve for the antisymmetric $m = 0$ mode is approaching that for $m = 1$, but it does not cross the latter, even by $T_m = 100,000$. The neutral stability curves for $m = 2$ and 3 are considerably higher. As already discussed for Fig. 1, for $Pr = 0.0286$, there is a switch from the $m = 1$ mode to the $m = 0$ mode at $T_m = 33,000$ and $Ra_{cr} = 5016$, while the neutral stability curve for $m = 2$ is above and nearly parallel to that for $m = 0$. For some value of Pr between 0.0286 and 0.2 , the neutral stability curve for $m = 2$ moves below that for $m = 0$. For $Pr = 0.2$, there is a switch from the $m = 1$ mode to the $m = 2$ mode at $T_m = 9300$ and $Ra_{cr} = 4710$, and there is another switch from the $m = 2$ mode to the $m = 3$ mode at $T_m = 45,000$ and $Ra_{cr} = 21,120$. For $Pr = 0.2$, $Ra_{cr} = 30,170$ at $T_m = 70,000$, while the neutral stability curve for $m = 0$

is above those for $m = 1, 2$ and 3 in Fig. 2. For $Pr = 1.0$, we stopped the calculations at $Ra_{cr} = 30,000$ and $T_m = 32,000$, and the critical mode is the $m = 1$ mode for this entire range. The neutral stability curve for the $m = 2$ mode comes very close to that for the critical $m = 1$ mode near $T_m = 5500$ and $Ra_{cr} = 6015.7$, but as T_m is increased further, the slope of the $m = 2$ curve increases so that this curve does not cross the $m = 1$ curve. Similarly, the $m = 3$ neutral stability curve comes very close to the $m = 1$ curve near $T_m = 10,000$ and $Ra_{cr} = 10,762$, but then it too rises more quickly and does not cross the $m = 1$ curve. For $Pr = 1.0$, the neutral stability curve for the $m = 0$ mode is well above that for the $m = 1$ mode. Clearly there is some change in the physics of the instability between (1) $Pr = 0.2$ where the $m = 2$ curve crosses the $m = 1$ curve and then the $m = 3$ curve crosses the $m = 2$ curve and (2) $Pr = 1.0$ where the $m = 2$ and 3 curves come close to the $m = 1$ curve but do not cross it, leaving $m = 1$ as the critical mode for the entire range considered here. Where the $m = 2$ or 3 curve comes close to the $m = 1$ curve for $Pr = 1.0$, the slow decay of both modes may mean that a nonlinear modal coupling leads to an $m = 2$ or 3 transition which cannot be predicted by the linear stability analysis. For $T_m = 5500$ and $Ra = 6015.7$, $\lambda = 58.577i$ for the $m = 1$ mode and $\lambda = -0.453 + 201.54i$ for the $m = 2$ mode. For $T_m = 10,000$ and $Ra = 10,762$, $\lambda = 92.29i$ for the $m = 1$ mode and $\lambda = -2.736 + 488.98i$ for the $m = 3$ mode. At both points, the natural frequencies of the two modes are not well matched.

Some physical insights into the stabilizing effects of an RMF and into the dependence of Ra_{cr} on Pr are provided by the characteristics of the base-state and of the perturbation variables for the critical mode. First we consider how the base-state differs from a simple superposition of the velocities driven by the RMF in an isothermal fluid, i.e., the same T_m with $Ra = 0$, and the pure-conduction horizontal isotherms for a stagnant fluid, i.e., the same Ra with $T_m = 0$. The primary difference is the change in the isotherms due to the meridional convection driven by the RMF. For $Pr = 0.001$, convective heat transfer is negligible compared to conduction, so that the isotherms remain horizontal and equally spaced for all $T_m < 70,000$. For $Pr = 0.0286$, there is a moderate deflection of the isotherms, and we have already noted that the axial heat flux at the liquid–solid interfaces becomes skewed toward $r = 1$. For $Pr = 0.2$ and 1.0 , the changes in the isotherms are much more significant. For example, the base-state isotherms for $Pr = 1.0$, $T_m = 26,000$ and $Ra_{cr} = 25,040.9$ are plotted in Fig. 3. Clearly this temperature distribution is very different from the pure-conduction temperature for the Rayleigh–Bénard problem without an RMF. The change in the base-state temperature distribution is one of the reasons that Ra_{cr} increases as Pr is increased for a given value of T_m .

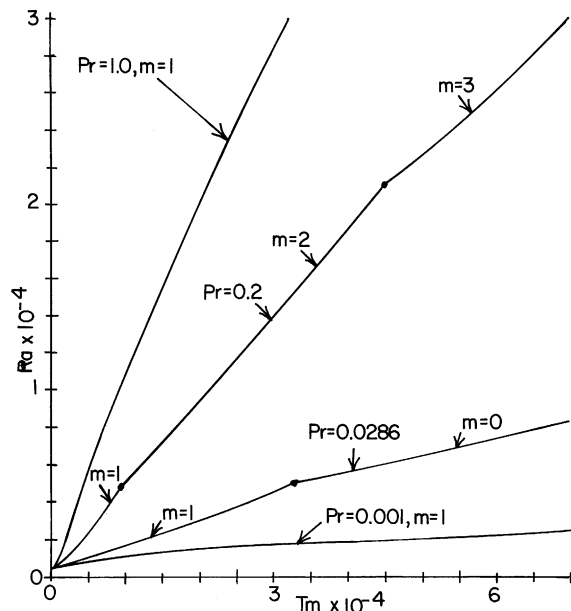


Fig. 2. Linear stability predictions of Ra_{cr} versus T_m for $Pr = 0.001, 0.0286, 0.2$ and 1.0 .

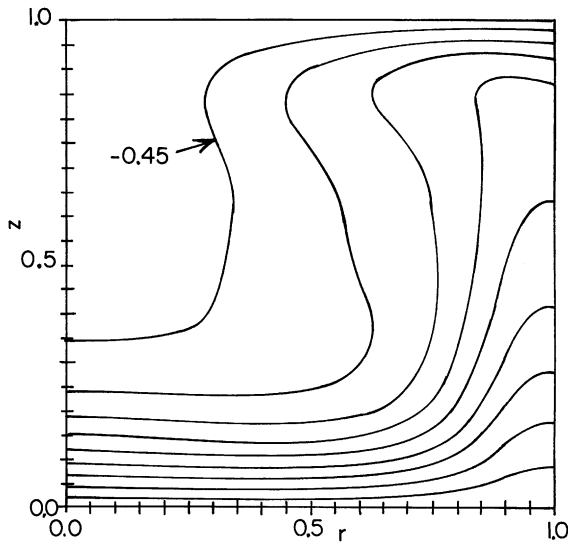


Fig. 3. Base-state isotherms for $Pr = 1.0$, $T_m = 26,000$ and $Ra_{cr} = 25,040.9$; $T_0 = -0.05k$, for $k = 1$ to 9 .

The non-zero values of $\partial T_0/\partial r$ created by the RMF should produce a buoyant convection which augments the meridional circulation driven by the RMF, but this change turns out to be small. For example, for the critical flows for $T_m = 8000$, the maximum values of the base-flow stream function are 3.767, 3.796, 4.04 and 3.959 for $Pr = 0.001, 0.0286, 0.2$ and 1.0 , respectively, while the corresponding values for $T_m = 20,000$ are 6.365, 6.455, 6.851 and 6.56. Davidson [8] showed that the maximum value of the azimuthal velocity driven by an RMF is determined by the balance between (1) the decrease of angular momentum due to viscous shear stresses as a fluid particle moves vertically and then radially inward inside the boundary layers adjacent to the fixed walls, and (2) the increase of angular momentum due to the RMF as the fluid particle crosses the inviscid central region from the top or bottom boundary layer to the vertical-wall boundary layer. Therefore an increase in the meridional circulation due to the buoyant force associated with the non-zero value of $\partial T_0/\partial r$ should reduce the time a particle spends crossing the inviscid central region and thus reduce the angular momentum it gains during this crossing. For $T_m = 8000$, the maximum values of the base-flow azimuthal velocity are 114.34, 113.91, 110.31 and 110.44 for $Pr = 0.001, 0.0286, 0.2$ and 1.0 , respectively, while the corresponding values for $T_m = 20,000$ are 230.08, 228.21, 220.64 and 223.9. In summary, for $Pr = 0.2$ and 1.0 , the base-state temperature distribution is significantly different from that for pure conduction, but the base-flow velocities are quite close to those for an isothermal fluid with the same RMF for all four values of Pr .

For $m \geq 1$, the perturbation variables for the critical mode have a constant spatial pattern which rotates in the $+\theta$ direction with the angular velocity λ_1/m . A key question is whether (1) this rotation of a constant pattern simply represents convection with some average of the base-flow azimuthal velocity or (2) there is some physical mechanism causing the perturbation pattern to rotate faster or slower than the base-flow azimuthal motion. The angular velocity of the base-flow, $v_{\theta 0}/r$, is not uniform over the cross-section. However, there is always a region of nearly rigid-body rotation near the origin, and its angular velocity is

$$\Omega_0 = \lim_{r \rightarrow 0} \left[\frac{v_{\theta 0}(r, 0)}{r} \right]. \tag{11}$$

For small values of T_m , the region of rigid-body rotation is small, but for $T_m > 10,000$, it occupies roughly $0 \leq r \leq 0.7, |z| \leq 0.5$. For these larger values of T_m , as r increases from 0.7 to 1.0 , the base-flow angular velocity decreases from Ω_0 to 0 , and as $|z|$ increases from 0.5 to 1.0 , the base-flow angular velocity first increases to roughly $1.5\Omega_0$ and then decreases to 0 . Thus the average base-flow angular velocity is close to Ω_0 . The values of λ_1 for the critical $m = 1$ mode for $Pr = 0.001, 0.0286, 0.2$ and 1.0 , as well as the value of Ω_0 , are plotted as a function of T_m in Fig. 4. As noted already, the values of $v_{\theta 0}$ are very nearly independent of Pr , so this is also true for Ω_0 . For all four values of Pr , λ_1 is significantly less than Ω_0 , so that some physical mechanism is causing the perturbation to rotate slower than the average base-flow angular velocity. There is clearly a competition between convection and conduction of the perturbation temperature. When conduction strongly dominates for $Pr = 0.001$, λ_1 for the $m = 1$ mode is very small, and the instability is nearly stationary. It appears that λ_1 for the $m = 1$ mode goes to zero as $Pr \rightarrow 0$ for all values of T_m . As Pr is increased, and the ratio of convection of T_1 to its conduction increases, λ_1 for the $m = 1$ mode increases. For gallium, with $Pr = 0.0286$, λ_1 is still far below Ω_0 . Even for $Pr = 1.0$, λ_1 for the $m = 1$ mode is still only slightly larger than $0.5\Omega_0$.

For the $m = 2$ and 3 modes, (λ_1/m) is closer to Ω_0 than it is for the $m = 1$ mode. For $Pr = 0.0286$ and $T_m = 39,630$, $(\lambda_1/m) = 93$ and 328 for the $m = 1$ and 2 modes, respectively, while $\Omega_0 = 467.5$. For $Pr = 0.2$, (λ_1/m) is very close to $0.75\Omega_0$ over the entire range of T_m where the $m = 2$ mode is critical, while (λ_1/m) is very close to $0.9\Omega_0$ over the entire range of T_m where the $m = 3$ mode is critical. Therefore the angular velocity of the $m = 1$ mode is much less than that of the base-flow azimuthal motion with a strong dependence on Pr , while the $m = 2$ and 3 modes have angular velocities which are still less than Ω_0 , but are much closer to Ω_0 .

Some physical insights into the results in Fig. 2 are provided by the difference between the azimuthal phase

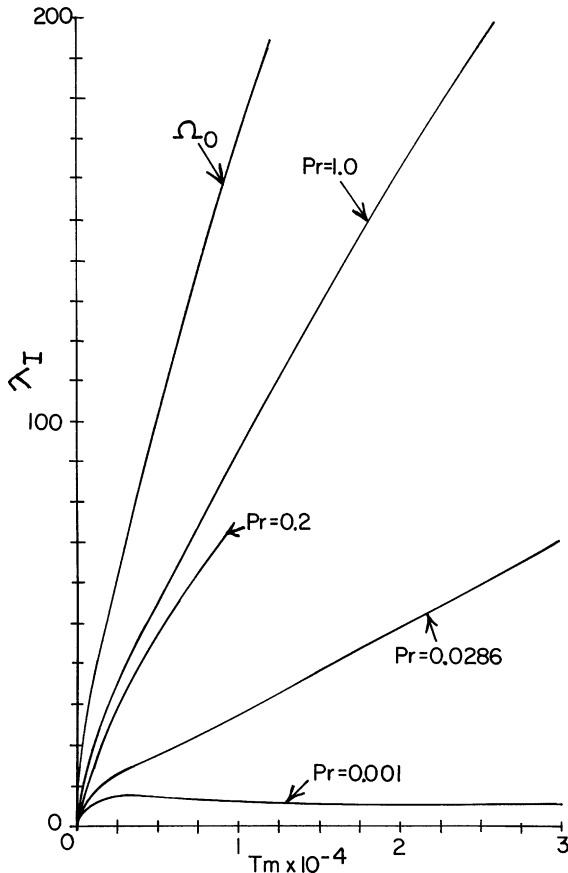


Fig. 4. Dimensionless frequency λ_1 for the critical $m = 1$ mode versus T_m for $Pr = 0.001, 0.0286, 0.2$ and 1.0 . Also the angular velocity Ω_0 of the base-flow rigid-body rotation near the origin.

shifts for the perturbation temperature and for the vertical perturbation velocity for $m \geq 1$. If we use a reference frame which is rotating around the z axis with the angular velocity λ_1/m , then the perturbation variables are independent of t for $m \geq 1$. In this rotating reference frame, the azimuthal coordinate is $\Theta = \theta - \lambda_1 t/m$ and the base-flow azimuthal velocity is $V_{\theta 0} = v_{\theta 0} - \lambda_1 r/m$. Eq. (9) for the temperature can be rewritten as

$$T = T_0(r, z) + \varepsilon \bar{T}_1(r, z) \cos\{m[\Theta - \Phi_T(r, z)]\}, \tag{12}$$

where

$$\bar{T}_1 = (T_{1R}^2 + T_{1I}^2)^{1/2} \tag{13}$$

and

$$\Phi_T = \frac{1}{m} \arctan\left(\frac{T_{1I}}{T_{1R}}\right) \tag{14}$$

are the amplitude and azimuthal phase shift for the perturbation temperature. At a given point (r, z) for $m = 1$, the maximum perturbation temperature occurs at

$\Theta = \Phi_T$, the minimum occurs at $\Theta = \Phi_T + \pi$, and the zeros occur at $\Theta = \Phi_T \pm \pi/2$. The Φ for each perturbation variable can vary considerably with (r, z) due to the azimuthal convection with $V_{\theta 0}(r, z)$ which varies from positive values in the central region to negative values near the walls. Here we focus on the difference between the azimuthal phase shifts for the perturbation temperature and for the vertical perturbation velocity,

$$\Delta\Phi = \Phi_T - \Phi_{v_z}, \tag{15}$$

where Φ_{v_z} is given by Eq. (14) with T_{1I} and T_{1R} replaced by v_{z1I} and v_{z1R} , respectively. For $Pr = 0.0286$ and $m = 1$, the values of $\Delta\Phi$ at $z = 0$ for $T_m = 1000, 8000, 14,000, 20,000$ and $30,000$ are plotted as functions of r in Fig. 5. For $T_m = 0$, $\Delta\Phi = 0$ everywhere and for all values of Pr . For $T_m = 1000$ and $Pr = 0.0286$, the variation of $\Delta\Phi$ with r arises because there is more convection of v_{z1} with $V_{\theta 0}$ than there is of T_1 because of the small value of Pr . Thus the maximum values of the vertical perturbation velocity are at a larger and smaller value of Θ than those of T_1 , near $r = 0$ and 1 , respectively. For $T_m \geq 8000$, $\Delta\Phi$ is positive for all values of r , and is increasing as T_m is increased. This means that the maximum value of T_1 is at a larger value of Θ than that of v_{z1} . The origin of this difference in phase shift is illustrated with some of the important terms in the perturbation version of Eq. (3),

$$\frac{V_{\theta 0}}{r} \frac{\partial T_1}{\partial \Theta} - Pr^{-1} \nabla^2 T_1 = -\frac{\partial T_0}{\partial z} v_{z1}. \tag{16}$$

The term on the right side of this equation is the primary source of perturbation temperature, namely a vertical perturbation velocity carries hotter fluid upward or colder fluid downward. The phase shift depends on the balance between the azimuthal convection term and the conduction term. Since the magnitude of $V_{\theta 0}$

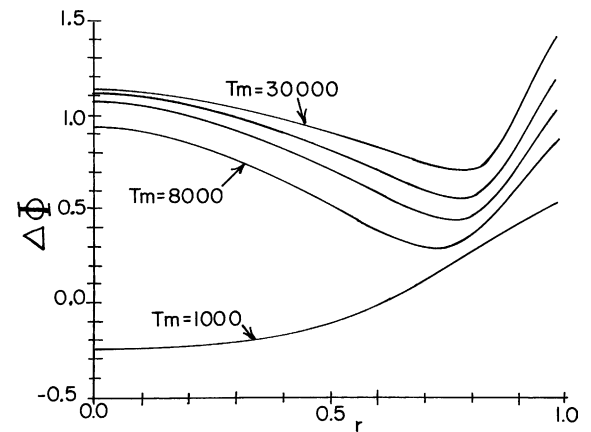


Fig. 5. Difference between the azimuthal phase shifts for the perturbation temperature and the axial perturbation velocity at $z = 0$ for the critical $m = 1$ mode, for $Pr = 0.0286$ and for $T_m = 1000, 8000, 14,000, 20,000$ and $30,000$.

increases as T_m is increased, the ratio of the azimuthal convection to conduction is characterized by $T_m^p Pr$, where p is a power which varies from 1.0 for small values of T_m to 0.67 for larger values of T_m [8]. For $T_m^p Pr \ll 1$, the azimuthal convection is much smaller than conduction, so that T_1 is in phase with v_{z1} and $\Delta\Phi = 0$. For $T_m^p Pr \gg 1$, conduction is much smaller than the azimuthal convection, and there is a phase shift of $\pi/2$ between T_1 and v_{z1} . Since $\partial T_0/\partial z < 0$, the direction of the phase shift depends on the sign of $V_{\theta 0}$ when azimuthal convection dominates. For $V_{\theta 0} > 0$, $\Delta\Phi = \pi/2$, i.e., if v_{z1} varies as $\cos \Theta$, then T_1 varies as $\sin \Theta$. If $V_{\theta 0} < 0$, $\Delta\Phi = -\pi/2$. In Fig. 5, $\Delta\Phi$ is positive and is approaching $\pi/2$ for all values of r as T_m is increased. There are two reasons why $\Delta\Phi$ does not change signs near $r = 1$. First, for $Pr = 0.0286$, λ_1 is much smaller than Ω_0 , so that the region near $r = 1$ where $V_{\theta 0} < 0$ is very small. Second, thermal conduction is certainly not small for $Pr = 0.0286$, so that the dominance of $V_{\theta 0} > 0$ for most values of r is carried by conduction to the small region near $r = 1$ where $V_{\theta 0} < 0$. On the other hand, for $Pr = 1.0$, $T_m = 14,000$, $m = 1$ and $Ra_{cr} = 14,539.4$, $\Delta\Phi$ at $z = 0$ decreases from 1.22 at $r = 0$ to 0.75 at $r = 0.62$, and then it plunges rather abruptly to -0.35 at $r = 0.7$, remaining nearly constant to $r = 1$. First, for $Pr = 1.0$, λ_1 is a little more than $0.5\Omega_0$, so that $V_{\theta 0} < 0$ for a much larger range near $r = 1$. Second, with $Pr = 1.0$, thermal conduction is weak enough that it cannot overwhelm the large radial temperature gradient produced by the azimuthal convection. Of course this discussion of the origin of the difference in phase shifts is very rough because many of the terms in the perturbation version of Eq. (3) which are not included in our discussion Eq. (16) are in fact quite important, particularly for $Pr = 1.0$ when the base-state temperature is far from that for pure conduction.

We believe that there is a correlation between (1) the $\Delta\Phi$ arising from the convection of the perturbation variables with the azimuthal base-flow velocity driven by the RMF, and (2) the increase of Ra_{cr} when either T_m or Pr are increased in Fig. 2. For the Rayleigh–Bénard instability for $T_m = 0$, $\Delta\Phi = 0$, so that v_{z1} is positive wherever T_1 is positive and v_{z1} is negative wherever T_1 is negative. Wherever there is upward flow, convective heat transfer produces an increase in temperature, so that buoyancy supports the upward flow, and wherever there is downward flow, convective heat transfer produces a decrease in temperature, so that buoyancy supports downward flow. Therefore convective heat transfer and buoyancy reinforce each other over the entire cross-section of the cylinder. When $\Delta\Phi \neq 0$, v_{z1} and T_1 have the same signs and thus reinforce each other for $\Delta\Theta = 2\pi - 2|\Delta\Phi|$, but v_{z1} and T_1 have opposite signs and thus oppose each other for $\Delta\Theta = 2|\Delta\Phi|$. Clearly as $|\Delta\Phi| \rightarrow \pi/2$, both the region of reinforcement and the region of opposition approach $\Delta\Theta = \pi$, which probably

means that $Ra_{cr} \rightarrow \infty$. As $|\Delta\Phi|$ increases, the temperature difference between the top and bottom walls must be increased so that reinforcement for $\Delta\Theta = 2\pi - 2|\Delta\Phi|$ can overcome the opposition for $\Delta\Theta = 2|\Delta\Phi|$ to produce the instability. Since $\Delta\Phi$ increases as $T_m^p Pr$, an increase of either Pr or T_m leads to an increase of Ra_{cr} . For the infinitely long cylinder, Volz and Mazuruk [12] also found that Ra_{cr} increased as either T_m or Pr was increased.

For $Pr = 0.0286$, a key element in our hypothesis about a nonlinear coupling between the $m = 0$ and 2 modes is the fact that the frequency of the $m = 0$ mode is roughly half that of the $m = 2$ mode. For $m \geq 1$, the periodicity is the result of the rotation of a spatially constant perturbation pattern with the angular velocity λ_1/m , i.e., the perturbation flow is steady in a rotating reference frame. The values of the perturbation variables indicate that the periodicity of the $m = 0$ mode arises from a coupling between the $v_{\theta 1}$ produced by the radial convection of the base-flow azimuthal velocity and the v_{r1} produced by the centrifugal force due to the azimuthal velocity. The contour plots of ψ_{1R} and ψ_{1I} for $Pr = 0.0286$, $T_m = 50,000$, $m = 0$ and $Ra_{cr} = 6466$ are presented in Fig. 6. From Eq. (9) for $\lambda_R = m = 0$, $\psi_1 = \psi_{1R}$ at $t = 0$, $\psi_1 = -\psi_{1I}$ at $t = \pi/2\lambda_1$, $\psi_1 = -\psi_{1R}$ at $t = \pi/\lambda_1$ and $\psi_1 = \psi_{1I}$ at $t = 3\pi/2\lambda_1$. Fig. 6a indicates that the counterclockwise meridional circulation at $t = 0$ consists of axially upward flow for $r > 0.6$, radially inward flow for $z > 0$, axially downward flow for $r < 0.6$ and radially outward flow for $z < 0$. At $t = 0$, the values of $v_{\theta 1}$ are relatively small and positive for $z > 0$. The radially inward flow for $z > 0$ convects the base-flow azimuthal velocity, as represented by $v_{r1}\partial(rv_{\theta 0})/\partial r$, causing the values of $v_{\theta 1}$ for $z > 0$ to increase during the quarter period $0 \leq t \leq \pi/2\lambda_1$. Thus at $t = \pi/2\lambda_1$, $v_{\theta 1}$ is positive for $z > 0$ and has a maximum value of 9.87 at $r = 0.3$ and $z = 0.87$. During this quarter period, the centrifugal force, as represented by $2v_{\theta 1}v_{\theta 0}/r$, has increased to positive values for $z > 0$ and has changed the meridional circulation, as reflected by $\psi_1 = -\psi_{1I}$ at $t = \pi/2\lambda_1$, with the contours of ψ_{1I} in Fig. 6b. The counterclockwise flow for $t = 0$ has been pushed up to roughly $z > 0.65$ and there is now a clockwise circulation for $|z| < 0.65$ with axially upward flow for $r < 0.7$ and axially downward flow for $r > 0.7$. From both meridional circulations, there is radially outward for $0 < z < 0.87$. The associated convection of base-flow azimuthal velocity begins to decrease the positive values of $v_{\theta 1}$ for $z > 0$. By $t = \pi/\lambda_1$, $v_{\theta 1}$ has small negative values over most of the cross-section for $z > 0$, and there is clockwise meridional flow over the entire cross-section. During the quarter period $\pi/\lambda_1 \leq t \leq 3\pi/2\lambda_1$ the radially outward flow for $z > 0$ convects the base-flow azimuthal velocity, producing large negative values of $v_{\theta 1}$ at $t = 3\pi/2\lambda_1$ for $z > 0$. The associated centrifugal force pushes the clockwise meridional circulation up to

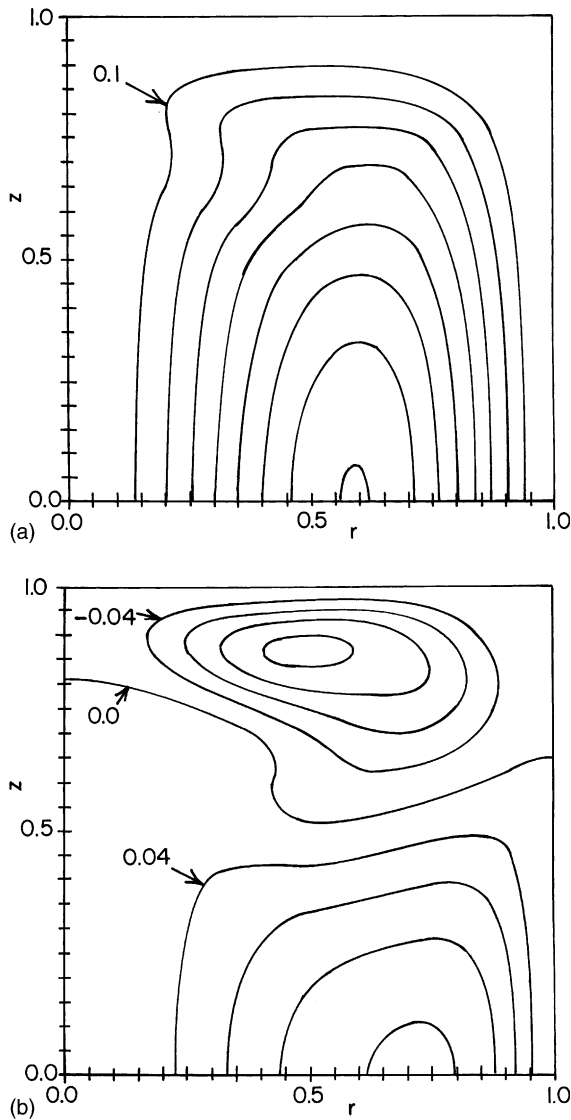


Fig. 6. Contour plots for the real and imaginary parts of the stream function for the perturbation meridional circulation for $Pr = 0.0286$, $T_m = 50,000$, $m = 0$ and $Ra_{cr} = 6466$ (a) $\psi_{1R} = 0.1k$, for $k = 1$ to 8. (b) $\psi_{1I}k$, for $k = -4$ to 4.

$z > 0.65$ and creates a counterclockwise circulation for $|z| < 0.65$. During the quarter period, $3\pi/2\lambda_1 \leq t \leq 2\pi/\lambda_1$, the values of v_{01} increase from their large negative values to small positive values and the counterclockwise circulation spread over the entire cross-section. While the periodicity of the $m = 0$ mode does not arise from convection with v_{00} , its frequency is still correlated with v_{00} since v_{00} and $\partial(rv_{00})/\partial r$ are the coefficients in the key terms for the centrifugal force and radial convection of base-flow angular momentum. For our typical case, $\lambda_1 = 364.92$ while the maximum value of v_{00} is 455.37.

4. Conclusions

A rotating magnetic field can lead to a large increase in the critical Rayleigh number Ra_{cr} for the initial transition from steady to periodic flow for the Rayleigh–Bénard instability. The value of Ra_{cr} increases as either the magnetic Taylor number T_m or the Prandtl number Pr is increased. For liquid gallium, the linear stability predictions for the $m = 1$ mode agree very well with previously published experimental measurements, but the experimental values of Ra_{cr} for the $m = 2$ mode are below the predictions of the linear stability analysis. There are characteristics of the $m = 0$ and 2 modes which support a hypothesis that this difference may arise from a nonlinear coupling of these two modes. For $m = 1$, the perturbation pattern of the critical mode rotates with an angular velocity which is less than that of the base-flow, where this difference arises from a competition between conductive and convective heat transfer for the perturbation temperature. As either Pr or T_m is increased, the azimuthal phase shift between the perturbation temperature and the axial perturbation velocity increases, and this increasing phase shift appears to be one reason for the increase in Ra_{cr} .

Acknowledgements

This research was supported by the National Science Foundation under Grant CTS-0129028 and by the National Aeronautics and Space Administration under Grant NAG 8-1705. The calculations were performed on a workstation donated by the International Business Machines Corporation. Drs. I. Grant and G. Gerbeth very generously provided additional data for their stability analysis [17] which was very helpful.

References

- [1] P. Dold, K.W. Benz, Rotating magnetic field: fluid flow and crystal growth applications, *Progr. Crystal Growth Charact. Mater.* 38 (1999) 7–38.
- [2] L. Martin Witkowski, P. Marty, Effect of a rotating magnetic field of arbitrary frequency on a liquid metal column, *Eur. J. Mech. B, Fluids* 17 (1998) 239–254.
- [3] K. Mazuruk, N. Ramachandran, M.P. Volz, D. Gillies, Study of frequency effects of a rotating magnetic field on fluid flow in vertical cylinders, *Materials Research in Low Gravity, Soc. Photo-optical Instrum. Eng., San Diego, CA* 3123, 1997, pp. 262–270.
- [4] L. Martin Witkowski, P. Marty, J.S. Walker, Multidomain analytical-numerical solution for a rotating magnetic field with a finite-length conducting cylinder, *IEEE Trans. Magn.* 36 (2000) 452–460.

- [5] L. Martin Witkowski, P. Marty, J.S. Walker, Liquid–metal flow in a finite-length cylinder with a high-frequency rotating magnetic field, *J. Fluid Mech.* 436 (2001) 131–143.
- [6] J.S. Walker, Bridgman crystal growth with a strong, low-frequency, rotating magnetic field, *J. Crystal Growth* 192 (1998) 318–327.
- [7] P.A. Davidson, J.C.R. Hunt, Swirling recirculating flow in a liquid–metal column generated by a rotating magnetic field, *J. Fluid Mech.* 185 (1987) 67–106.
- [8] P.A. Davidson, Swirling flow in an axisymmetric cavity of arbitrary profile, driven by a rotating magnetic field, *J. Fluid Mech.* 245 (1992) 669–699.
- [9] L. Martin Witkowski, J.S. Walker, P. Marty, Nonaxisymmetric flow in a finite-length cylinder with a rotating magnetic field, *Phys. Fluids* 11 (1999) 1821–1826.
- [10] M.P. Volz, K. Mazuruk, An experimental study of the influence of a rotating magnetic field on Rayleigh–Bénard convection, *J. Fluid Mech.* 444 (2001) 79–98.
- [11] J.C. Buell, I. Catton, Effect of rotation on the stability of a bounded cylindrical layer of fluid heated from below, *Phys. Fluids* 26 (1983) 892–896.
- [12] M.P. Volz, K. Mazuruk, Thermoconvective instability in a rotating magnetic field, *Int. J. Heat Mass Transfer* 42 (1999) 1037–1045.
- [13] B.T. Smith, et al., *Matrix Eigensystem Routines—EISPACK Guide*, second ed., Vol. 6 of *Lecture Notes in Computer Science*, Springer, NY, 1976.
- [14] Y. Saad, *Numerical Methods for Large Eigenvalue Problems*, Manchester University Press Series in Algorithms and Architectures for Advanced Scientific Computing, 1991.
- [15] R. Touihri, H. BenHadid, D. Henry, On the onset of convective instabilities in cylindrical cavities heated from below. I. Pure thermal case, *Phys. Fluids* 11 (1999) 2078–2088.
- [16] G. Neumann, Three-dimensional numerical simulation of buoyancy-driven convection in vertical cylinders heated from below, *J. Fluid Mech.* 214 (1990) 559–578.
- [17] I. Grants, G. Gerbeth, Linear three-dimensional instability of a magnetically driven rotating flow, *J. Fluid Mech.* 463 (2002) 229–239.